Impedance Analysis of Voltage Source Converter Using Direct Power Control

Gao, Shuning; Zhao, Haoran; Gui, Yonghao; Luo, Jia; Blaabjerg, Frede

Published in:
I E E E Transactions on Energy Conversion

DOI (link to publication from Publisher):
10.1109/TEC.2020.3020181

Publication date:
2021

Document Version
Accepted author manuscript, peer reviewed version

Impedance Analysis of Voltage Source Converter Using Direct Power Control

Shuning Gao, *Student Member, IEEE*, Haoran Zhao, *Senior Member, IEEE*, Yonghao Gui, *Senior Member, IEEE*, Jia Luo, *Student Member, IEEE* and Frede Blaabjerg, *Fellow, IEEE*

***Abstract*—The impedance analysis has been proposed and proved to be an effective way to analyze the grid-connected stability of Voltage Source Converter (VSC) based energy conversion systems. Most of the existing impedance analyzes are discussed based on vector oriented control, while there are few discussions about the impedance analysis of Direct Power Control (DPC). In this paper, an impedance modeling approach of VSC using the DPC is firstly proposed and analyzed, which fills the gap of impedance analysis of the DPC based converters and provides a basis for studying the corresponding grid-integration stability problems. Since there is no need for PLL and Park transformation, the impedance matrix is built directly using the $\alpha\beta$ reference frame and features symmetrical characteristics. The proposed impedance matrix can be transformed into a positive-sequence impedance and analyzed by using SISO Nyquist criteria. The stability of a weak-grid connected VSC using DPC is analyzed in this paper. The main factors affecting system stability, including the grid and control parameters, are considered in the analysis. The effectiveness of the proposed method is demonstrated by the simulations carried out in the Matlab/Simulink Simscape Power Systems as well as a hardware-in-loop system.**

***Index Terms*—Direct power control, impedance model, voltage source converter, stability, weak grid.**

I. Introduction

NOWADAYS, an increasing amount of renewable energy sources have been largely integrated into modern power systems through power electronic equipments such as Voltage Source Converters (VSCs) [1]. Such equipments improve the controllability of the power grid. However, there are possible instabilities hidden inside the dynamic interaction between the actively controlled VSCs and the passive devices in the system [2]. Therefore, it is crucial to study the specific mechanism of the dynamic interaction in order to avoid the potential stability problems and guarantee a stable operation.

Recently, many studies have addressed the stability issues of grid-connected VSCs using impedance analysis, which is a research hotspot and has been widely discussed, e.g. in [3]–[7]. The impedance model and frequency-domain stability analysis of the VSC-based HVDC system, photovoltic inverter, type-III and type-IV wind turbines, have been proposed and thoroughly discussed [8]–[13]. The mainstream control strategies for VSC can be classified into Vector Oriented Control (VOC) and Direct Power Control (DPC). However, most of the papers about impedance analysis only focus on the controller designed based on VOC.

The VOC usually requires a Phase-Locked-Loop (PLL) for grid-synchronization and transforms the three-phase ac signals into dc components in the dq-reference frame for the subsequent control. The dynamics of the PLL have a significant influence on the frequency-domain characteristic. Due to the highly non-linear characteristic of the PLL and outer power control loop, the impedance modeling of VSCs with VOC requires small-signal analysis near the point of operation [14]. Moreover, the impedance matrix of grid-connected VSC using conventional VOC is asymmetric, which brings a frequency coupling phenomenon [15], [16]. The asymmetric system can be presented by a multi-input multi-output (MIMO) transfer matrix, which is not easy to analyze [17]. A number of studies have suggested using various impedance models in different domains, such as sequence domain, or phasor domain, to reduce the coupling and simplify the analysis [15], [16], [18]. Recently, a symmetrical PLL is proposed in [19], which eliminates frequency-coupling terms and enhances the system stability under a weak grid condition. A symmetrical admittance modeling for grid-connected VSC is proposed in [18]. However, the frequency-coupling effect is not investigated. A complex-valued impedance modeling for VSC in the stationary frame is proposed in [20], which reveals the frequency-coupling effect of the ac-dc dynamics interaction. But the corresponding stability analysis criterion is missing. An impedance measurement method using an off-shelf frequency response analyzer is proposed in [21], which demonstrates that the accuracy of stability analysis of VOC based method is greatly affected by the frequency coupling phenomenon. Although the impedance analysis for VOC has been thoroughly discussed, only few studies have been seen about impedance analysis for other typical control strategies, e.g., DPC.

The DPC has been proposed for years [22]–[29]. It has fast transient dynamics and usually does not need grid synchronization. However, the switching frequency of a typical DPC method is non-constant with a hysteresis chosen based on a prede fined Look-Up-Table (LUT) [22]. The non-linear structure with non-constant switching frequency brings difficulties to find the frequency-domain impedance and analyze

This work was supported by the National Key R&D Program of China (2018YFB0904004) *(Corresponding author: Haoran Zhao).*

S. Gao is with the School of Electrical Engineering, Shandong University, Jinan 250061, China, and was also with the Automation & Control Section at the Department of Electronic Systems, Aalborg University, 9220 Aalborg, Denmark (email:gaosn@mail.sdu.edu.cn).

H. Zhao and J. Luo are with the School of Electrical Engineering, Shandong University, Ji'nan 250061, China (email:hzhao@sdu.edu.cn, jialuo@mail.sdu.edu.cn).

Y. Gui is with Automation & Control Section, Department of Electronic Systems, Aalborg University, 9220 Aalborg, Denmark (e-mail:yg@es.aau.dk).

F. Blaabjerg is with Department of Energy Technology, Aalborg University, 9220 Aalborg, Denmark (e-mail:fbl@et.aau.dk).

its small-signal stability. Recently, some studies have proposed to combine the DPC strategy with Pulse Width Modulation (PWM), which obtains a constant switching frequency [23]. Sliding Mode Control (SMC)-DPC [24], [29] and passivity-based control (PBC)-DPC [25] were designed for VSCs, which improves the system robustness against parameter mismatch. However, the SMC-DPC usually brings power chattering problem. The highly non-linear characteristic of SMC-DPC and PBC-DPC also makes the corresponding impedance model hard to be deduced.

This paper aims to present a newly-designed impedance analysis method for VSCs operating with the DPC method. The proposed method reveals the harmonic interaction between grid-connected VSC using DPC and the grid impedance. It provides a guide to the parameter design of the VSC under grid-connected condition. A newly proposed Voltage-Modulated (VM)-DPC presented in [30] is studied. One essential advantage of the VM-DPC is that it can transform the closed-loop VSC system into a Linear-Time-Invariant (LTI) one, which can be analyzed and designed through linear control techniques [30], [31]. It has a satisfactory steady-state performance and fast transient response [26], [30]–[34]. An linearization method is proposed to establish the impedance matrix of the VSC controlled by VM-DPC. Since the PLL and Park transformation are not included, their dynamics are not considered in the impedance modeling. The impedance matrix is built directly under $\alpha\beta$ reference frame and features symmetrical characteristics. Finally, the impedance matrix is transformed into a positive-sequence impedance model, and the stability of the system is estimated by using the SISO Nyquist stability criteria. The frequency-response accuracy of the proposed impedance model is verified through the frequency scanning method. The effects of the control parameters of the DPC and the Short-Circuit Ratio (SCR) of the weak grid on the system stability are also studied by the proposed impedance analysis. Simulations and Hardware-In-Loop (HIL) tests are carried out to verify the effectiveness of the proposed method.

The rest of this paper is organized as follows: the mathematical model and design of VSC with VM-DPC are introduced in Section II. The impedance modeling approach of the VM-DPC based VSC is presented in Section III. The stability criterion of VSC using VM-DPC is presented in Section IV and simulation results using MATLAB/Simulink Simscape Power Systems are shown in Section V. HIL test performed on RTDS is presented in Section VI, and finally the conclusions are drawn in the last section.

II. Basic Knowledge of VSC with VM-DPC

In this section, the basic mathematical model and design of the VM-DPC is introduced. The dc-link voltage (v_{dc}) is considered as a constant value in this paper. The grid impedance is a typical RLC-type grid impedance. The voltage and current are measured at the Point of Common Coupling (PCC) as the inputs of VM-DPC.

Referring to Fig. 1, the voltage-current relation of the grid-connected VSC system can be written as follows,

$$\boldsymbol{v}_{\mathrm{s}} = R_{\mathrm{g}}\boldsymbol{i}_{\mathrm{s}} + L_{\mathrm{g}}\frac{\mathrm{d}\boldsymbol{i}_{\mathrm{s}}}{\mathrm{d}t} + \boldsymbol{v}_{\mathrm{c}}, \tag{1}$$

where the bold letter denote the complex space vectors as, $\boldsymbol{v}_{\mathrm{s}} = v_{\mathrm{s}\alpha} + jv_{\mathrm{s}\beta}$. $\boldsymbol{i}_{\mathrm{s}} = i_{\mathrm{s}\alpha} + ji_{\mathrm{s}\beta}$ is the input current of VSC. $\boldsymbol{v}_{\mathrm{c}} = v_{\mathrm{c}\alpha} + jv_{\mathrm{c}\beta}$ is the controlled terminal voltage of VSC. R_{g} and L_{g} are the resistance and inductance of VSC respectively. Consider an inverter with a default output power, the active power P_{s} and reactive power Q_{s} can be calculated by,

$$P_{\mathrm{s}} + jQ_{\mathrm{s}} = -\frac{3}{2}\boldsymbol{v}_{\mathrm{s}} \cdot \boldsymbol{i}_{\mathrm{s}}^{*}. \tag{2}$$

The derivation of the instantaneous active and reactive power can be written based on (2) as follows,

$$\begin{cases} \dfrac{\mathrm{d}P_{\mathrm{s}}}{\mathrm{d}t} = -\dfrac{3}{2}(\dfrac{\mathrm{d}v_{\mathrm{s}\alpha}}{\mathrm{d}t}i_{\mathrm{s}\alpha} + \dfrac{\mathrm{d}i_{\mathrm{s}\alpha}}{\mathrm{d}t}v_{\mathrm{s}\alpha} + \dfrac{\mathrm{d}v_{\mathrm{s}\beta}}{\mathrm{d}t}i_{\mathrm{s}\beta} + \dfrac{\mathrm{d}i_{\mathrm{s}\beta}}{\mathrm{d}t}v_{\mathrm{s}\beta}) \\ \dfrac{\mathrm{d}Q_{\mathrm{s}}}{\mathrm{d}t} = -\dfrac{3}{2}(\dfrac{\mathrm{d}v_{\mathrm{s}\beta}}{\mathrm{d}t}i_{\mathrm{s}\alpha} + \dfrac{\mathrm{d}i_{\mathrm{s}\alpha}}{\mathrm{d}t}v_{\mathrm{s}\beta} - \dfrac{\mathrm{d}v_{\mathrm{s}\alpha}}{\mathrm{d}t}i_{\mathrm{s}\beta} - \dfrac{\mathrm{d}i_{\mathrm{s}\beta}}{\mathrm{d}t}v_{\mathrm{s}\alpha}) \end{cases}. \tag{3}$$

The design of the controller is based on an ideal grid voltage with angular frequency ω_{s} and the voltage can be expressed as follows, $v_{\mathrm{s}\alpha} = |v_{\mathrm{s}}|\cos(\omega_{\mathrm{s}}\mathrm{t} + \theta_0), \mathrm{v}_{\mathrm{s}\beta} = |\mathrm{v}_{\mathrm{s}}|\sin(\omega_{\mathrm{s}}\mathrm{t} + \theta_0)$. The instantaneous grid voltage variation can be expressed as,

$$\begin{cases} \dfrac{\mathrm{d}v_{\mathrm{s}\alpha}}{\mathrm{d}t} = -\omega_{\mathrm{s}}v_{\mathrm{s}\beta} \\ \dfrac{\mathrm{d}v_{\mathrm{s}\beta}}{\mathrm{d}t} = \omega_{\mathrm{s}}v_{\mathrm{s}\alpha} \end{cases}. \tag{4}$$

Substituting (4) and (1) into (3), the dynamics of the system can be established as follows,

$$\begin{cases} \dfrac{\mathrm{d}P_{\mathrm{s}}}{\mathrm{d}t} = -\omega_{\mathrm{s}}Q_{\mathrm{s}} - \dfrac{R_{\mathrm{g}}}{L_{\mathrm{g}}}P_{\mathrm{s}} + \dfrac{3}{2L_{\mathrm{g}}}\underbrace{[(v_{\mathrm{s}\alpha}v_{\mathrm{c}\alpha} + v_{\mathrm{s}\beta}v_{\mathrm{c}\beta}) - |v_{\mathrm{s}}^2|]}_{U_{\mathrm{P}}} \\ \dfrac{\mathrm{d}Q_{\mathrm{s}}}{\mathrm{d}t} = -\dfrac{R_{\mathrm{g}}}{L_{\mathrm{g}}}Q_{\mathrm{s}} + \omega_{\mathrm{s}}P_{\mathrm{s}} + \dfrac{3}{2L_{\mathrm{g}}}\underbrace{(v_{\mathrm{s}\beta}v_{\mathrm{c}\alpha} - v_{\mathrm{s}\alpha}v_{\mathrm{c}\beta})}_{U_{\mathrm{Q}}} \end{cases}, \tag{5}$$

where U_{P} and U_{Q} denotes the non-linear Voltage Regulation Terms (VRT) which contain coupling between $\boldsymbol{v}_{\mathrm{c}}$ and $\boldsymbol{v}_{\mathrm{s}}$. To reduce the influence of harmonic distortion on the control effect, a Band-Pass filter (BPF) is adopted in VM-DPC. The transfer function of BPF can be defined in the s-domain using Laplace transform as follows,

$$F_{\mathrm{f}}(s) = \frac{s^2}{s^2 + 2\zeta_{\mathrm{f}}\omega_{\mathrm{fn}}s + \omega_{\mathrm{fn}}^2}, \tag{6}$$

where ω_{fn} and ζ_{f} defines the natural frequency and damping ratio of BPF. In this paper, the ω_{fn} is chosen as $\omega_{\mathrm{fn}} = \omega_{\mathrm{s}}$. Therefore, $|F_{\mathrm{f}}(j\omega_{\mathrm{s}})| = 1$, $\angle F_{\mathrm{f}}(j\omega_{\mathrm{s}}) = 0°$. With the BPF, the voltage inputs of the controller can be written in the s-domain as $v'_{\mathrm{s}\alpha} = F_{\mathrm{f}}(s)v_{\mathrm{s}\alpha}$, $v'_{\mathrm{s}\beta} = F_{\mathrm{f}}(s)v_{\mathrm{s}\beta}$. The apostrophes denote the control signals through the BPF.

The calculation of the instantaneous active and reactive powers for VM-DPC can be expressed as follows [35],

$$\begin{cases} P'_{\mathrm{s}} = -\dfrac{3}{2}(v'_{\mathrm{s}\alpha}i_{\mathrm{s}\alpha} + v'_{\mathrm{s}\beta}i_{\mathrm{s}\beta}) \\ Q'_{\mathrm{s}} = -\dfrac{3}{2}(v'_{\mathrm{s}\beta}i_{\mathrm{s}\alpha} - v'_{\mathrm{s}\alpha}i_{\mathrm{s}\beta}) \end{cases}. \tag{7}$$

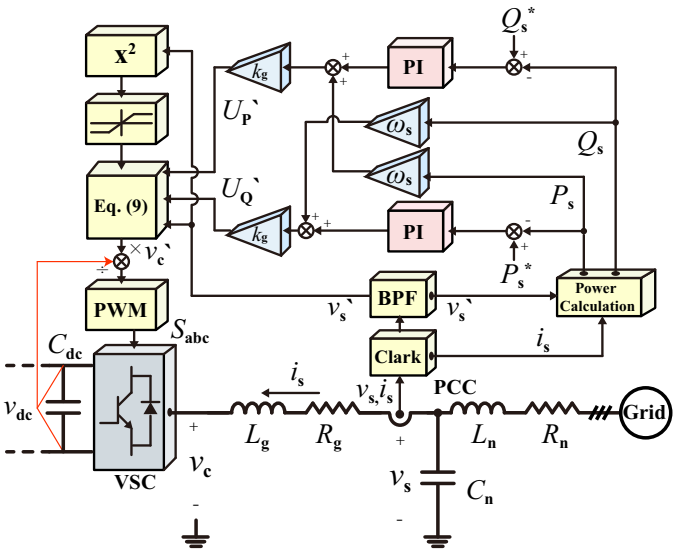

Fig. 1. Diagram of three-phase grid connected VSC using VM-DPC.

Since there is an apparent linear relation between the VRT and power components shown in (5), there are multiple methods that can be used to generate VRT. In order to cancel the coupling terms between active and reactive control loop in (5), a simple feed-forward compensator with a Proportional-Integral (PI) controller is used in this paper [26]. Considering the effect of BPF, the VRT can be redesigned as follows,

$$\begin{cases} U'_{\mathrm{P}} = \dfrac{2L_{\mathrm{g}}}{3}[K_{\mathrm{p}}(P_{\mathrm{s}}^{\mathrm{ref}} - P'_{\mathrm{s}}) + K_{\mathrm{i}}\displaystyle\int(P_{\mathrm{s}}^{\mathrm{ref}} - P'_{\mathrm{s}})\mathrm{d}t + \omega_{\mathrm{s}}Q'_{\mathrm{s}}] \\ U'_{\mathrm{Q}} = \dfrac{2L_{\mathrm{g}}}{3}[K_{\mathrm{p}}(Q_{\mathrm{s}}^{\mathrm{ref}} - q'_{\mathrm{s}}) + K_{\mathrm{i}}\displaystyle\int(Q_{\mathrm{s}}^{\mathrm{ref}} - Q'_{\mathrm{s}})\mathrm{d}t - \omega_{\mathrm{s}}P'_{\mathrm{s}}] \end{cases}. \tag{8}$$

In an ideal grid condition, the effect of the filter on the control can be ignored, i.e., $\boldsymbol{v}'_{\mathrm{s}} = \boldsymbol{v}_{\mathrm{s}}$, $P_{\mathrm{s}} = P'_{\mathrm{s}}$, $Q_{\mathrm{s}} = Q'_{\mathrm{s}}$. Therefore, by substituting (8) into (5), the closed-loop system can be represented by a second-order transfer function as follows,

$$\frac{P_{\mathrm{s}}}{P_{\mathrm{s}}^*} = \frac{Q_{\mathrm{s}}}{Q_{\mathrm{s}}^*} = \frac{K_{\mathrm{p}}s + K_{\mathrm{i}}}{s^2 + (-\frac{R_{\mathrm{g}}}{L_{\mathrm{g}}} + K_{\mathrm{p}})s + K_{\mathrm{ri}}}. \tag{9}$$

Selecting proper controller gains can make the closed-loop system globally exponentially stable [26]. Finally, by using the inverse transformation of (5), the controlled $\boldsymbol{v}'_{\mathrm{c}}$ can be calculated as,

$$\begin{cases} v'_{\mathrm{c}\alpha} = \dfrac{v'_{\mathrm{s}\alpha}U'_{\mathrm{P}} + v'_{\mathrm{s}\beta}U'_{\mathrm{Q}}}{|\boldsymbol{v}'_{\mathrm{s}}|^2} + v'_{\mathrm{s}\alpha} \\ v'_{\mathrm{c}\beta} = \dfrac{v'_{\mathrm{s}\beta}U'_{\mathrm{P}} - v'_{\mathrm{s}\alpha}U'_{\mathrm{Q}}}{|\boldsymbol{v}'_{\mathrm{s}}|^2} + v'_{\mathrm{s}\beta} \end{cases}, \tag{10}$$

where $|\boldsymbol{v}'_{\mathrm{s}}|^2$ can be calculated as ${v'_{\mathrm{s}\alpha}}^2 + {v'_{\mathrm{s}\beta}}^2$. The control block diagram of the method proposed in this paper is presented in details in Fig. 1.

III. Impedance Modeling of VM-DPC Based VSC

In this section, the impedance model of VM-DPC based VSC is developed. The proposed model indicates the closed-loop relation between $\boldsymbol{v}_{\mathrm{s}}$ and $\boldsymbol{i}_{\mathrm{s}}$. To establish the impedance model, the dynamics of the controlled terminal voltage $\boldsymbol{v}_{\mathrm{c}}$ in terms of $\boldsymbol{v}_{\mathrm{s}}$ and $\boldsymbol{i}_{\mathrm{s}}$ under $\alpha\beta$ reference frame should be deduced first. By substituting (8) into (10), the terminal voltage can be written as follows,

$$\begin{cases} v'_{\mathrm{c}\alpha} = L_{\mathrm{g}}(K_{\mathrm{p}}(A_\alpha + B_\alpha) + K_{\mathrm{i}}D_\alpha + C_\alpha) + v'_{\mathrm{s}\alpha} \\ v'_{\mathrm{c}\beta} = L_{\mathrm{g}}(K_{\mathrm{p}}(A_\beta + B_\beta) + K_{\mathrm{i}}D_\beta + C_\beta) + v'_{\mathrm{s}\beta} \end{cases}, \tag{11}$$

where $A_\alpha, A_\beta, B_\alpha, B_\beta, C_\alpha$ and C_β are four different coupling terms, D_α and D_β are the integral coupling terms, which can be written as,

$$\begin{aligned} A_\alpha &= -\frac{2(P'_{\mathrm{s}}v'_{\mathrm{s}\alpha} + Q'_{\mathrm{s}}v'_{\mathrm{s}\beta})}{3|\boldsymbol{v}'_{\mathrm{s}}|^2},\ A_\beta = -\frac{2(P'_{\mathrm{s}}v'_{\mathrm{s}\beta} - Q'_{\mathrm{s}}v'_{\mathrm{s}\alpha})}{3|\boldsymbol{v}'_{\mathrm{s}}|^2} \\ B_\alpha &= \frac{2(P_{\mathrm{ref}}v'_{\mathrm{s}\alpha} + Q_{\mathrm{ref}}v'_{\mathrm{s}\beta})}{3|\boldsymbol{v}'_{\mathrm{s}}|^2}, B_\beta = \frac{2(P_{\mathrm{ref}}v'_{\mathrm{s}\beta} - Q_{\mathrm{ref}}v'_{\mathrm{s}\alpha})}{3|\boldsymbol{v}'_{\mathrm{s}}|^2} \\ C_\alpha &= -\frac{2\omega_{\mathrm{s}}(P'_{\mathrm{s}}v'_{\mathrm{s}\beta} - Q_{\mathrm{s}}v'_{\mathrm{s}\alpha})}{3|\boldsymbol{v}'_{\mathrm{s}}|^2}, C_\beta = \frac{2\omega_{\mathrm{s}}(Q'_{\mathrm{s}}v'_{\mathrm{s}\beta} + P_{\mathrm{s}}v'_{\mathrm{s}\alpha})}{3|\boldsymbol{v}'_{\mathrm{s}}|^2} \end{aligned}. \tag{12}$$

$$\begin{aligned} D_\alpha &= \frac{2v'_{\mathrm{s}\alpha}}{3|\boldsymbol{v}'_{\mathrm{s}}|^2}\int(P_{\mathrm{sref}} - P'_{\mathrm{s}}) + \frac{2v'_{\mathrm{s}\beta}}{3|\boldsymbol{v}'_{\mathrm{s}}|^2}\int(Q_{\mathrm{sref}} - Q'_{\mathrm{s}}) \\ D_\beta &= \frac{2v'_{\mathrm{s}\beta}}{3|\boldsymbol{v}'_{\mathrm{s}}|^2}\int(P_{\mathrm{sref}} - P'_{\mathrm{s}}) - \frac{2v'_{\mathrm{s}\alpha}}{3|\boldsymbol{v}'_{\mathrm{s}}|^2}\int(Q_{\mathrm{sref}} - Q'_{\mathrm{s}}) \end{aligned}. \tag{13}$$

Substituting (7) into (12), it can be found that $A_\alpha, A_\beta, C_\alpha$ and C_β can be further simplified, which can be written as follows,

$$\begin{aligned} A_\alpha &= i_{\mathrm{s}\alpha},\ A_\beta = i_{\mathrm{s}\beta} \\ C_\alpha &= \omega_{\mathrm{s}}i_{\mathrm{s}\beta},\ C_\beta = -\omega_{\mathrm{s}}i_{\mathrm{s}\alpha} \end{aligned}. \tag{14}$$

However, $B_\alpha, B_\beta, D_\alpha$ and D_β are non-linear terms, which cannot be directly linearized. Therefore, in this paper, an linearization method for these terms are designed for the impedance modeling.

A. Approximation for $B_\alpha, B_\beta, D_\alpha$ and D_β

The harmonic contaminated grid voltage $\boldsymbol{v}_{\mathrm{s}}$ and current $\boldsymbol{i}_{\mathrm{s}}$ can be expressed by the sum of their fundamental components $\boldsymbol{v}_{\mathrm{sb}} = v_{\mathrm{s}\alpha\mathrm{b}} + jv_{\mathrm{s}\beta\mathrm{b}}$, $\boldsymbol{i}_{\mathrm{sb}} = i_{\mathrm{s}\alpha\mathrm{b}} + ji_{\mathrm{s}\beta\mathrm{b}}$ and harmonic components $\boldsymbol{v}_{\mathrm{sh}} = v_{\mathrm{s}\alpha h} + jv_{\mathrm{s}\beta h}$, $\boldsymbol{i}_{\mathrm{sh}} = i_{\mathrm{s}\alpha h} + ji_{\mathrm{s}\beta h}$, respectively. The expression of the inputs $\boldsymbol{v}'_{\mathrm{s}}$ and $\boldsymbol{i}_{\mathrm{s}}$ can be written as follows,

$$\begin{aligned} \boldsymbol{v}'_{\mathrm{s}} &= \boldsymbol{v}_{\mathrm{sb}} + \boldsymbol{v}'_{sh} \\ &= \underbrace{v_{\mathrm{s}\alpha\mathrm{b}} + \sum_{\mathrm{h}=1}^{N} F_{\mathrm{f}}(j\omega_{\mathrm{h}})v_{\mathrm{s}\alpha\mathrm{h}}}_{v'_{\mathrm{s}\alpha}} + j\underbrace{(v_{\mathrm{s}\beta\mathrm{b}} + \sum_{\mathrm{h}=1}^{N} F_{\mathrm{f}}(j\omega_{\mathrm{h}})v_{\mathrm{s}\beta\mathrm{h}})}_{v'_{\mathrm{s}\beta}} \\ \boldsymbol{i}_{\mathrm{s}} &= \boldsymbol{i}_{\mathrm{sb}} + \boldsymbol{i}_{\mathrm{sh}} \\ &= \underbrace{i_{\mathrm{s}\alpha\mathrm{b}} + \sum_{\mathrm{h}=1}^{N} i_{\mathrm{s}\alpha\mathrm{h}}}_{i_{\mathrm{s}\alpha}} + j\underbrace{(i_{\mathrm{s}\beta\mathrm{b}} + \sum_{\mathrm{h}=1}^{N} i_{\mathrm{s}\beta\mathrm{h}})}_{i_{\mathrm{s}\beta}} \end{aligned}, \tag{15}$$

where N is the number of total harmonic terms of the system. The subscripts h and b denote the harmonic and fundamental

$$\begin{cases}\sum_{\mathrm{h}=1}^{N} v_{\mathrm{c}\alpha\mathrm{h}} = L_{\mathrm{g}}[K_{\mathrm{p}}(\sum_{\mathrm{h}=1}^{N} i_{\mathrm{s}\alpha\mathrm{h}} + \frac{2P_{\mathrm{ref}}}{3v_{\mathrm{sb2}}}\sum_{\mathrm{h}=1}^{N} F_{\mathrm{f}} v_{\mathrm{s}\alpha\mathrm{h}} + \frac{2Q_{\mathrm{ref}}}{3v_{\mathrm{sb2}}}\sum_{\mathrm{h}=1}^{N} F_{\mathrm{f}} v_{\mathrm{s}\beta\mathrm{h}}) - K_{\mathrm{i}}\sum_{\mathrm{h}=1}^{N}\frac{i_{\mathrm{s}\beta\mathrm{h}}}{\omega_{\mathrm{s}}-\omega_{\mathrm{h}}} + \omega_{\mathrm{s}}\sum_{\mathrm{h}=1}^{N} i_{\mathrm{s}\beta\mathrm{h}}) + \sum_{\mathrm{h}=1}^{N} F_{\mathrm{f}} v_{\mathrm{s}\alpha\mathrm{h}} \\ \sum_{\mathrm{h}=1}^{N} v_{\mathrm{c}\beta\mathrm{h}} = L_{\mathrm{g}}[K_{\mathrm{p}}(\sum_{\mathrm{h}=1}^{N} i_{\mathrm{s}\beta\mathrm{h}} + \frac{2P_{\mathrm{ref}}}{3v_{\mathrm{sb2}}}\sum_{\mathrm{h}=1}^{N} F_{\mathrm{f}} v_{\mathrm{s}\beta\mathrm{h}} - \frac{2Q_{\mathrm{ref}}}{3v_{\mathrm{sb2}}}\sum_{\mathrm{h}=1}^{N} F_{\mathrm{f}} v_{\mathrm{s}\alpha\mathrm{h}}) + K_{\mathrm{i}}\sum_{\mathrm{h}=1}^{N}\frac{i_{\mathrm{s}\alpha\mathrm{h}}}{\omega_{\mathrm{s}}-\omega_{\mathrm{h}}} - \omega_{\mathrm{s}}\sum_{\mathrm{h}=1}^{N} i_{\mathrm{s}\beta\mathrm{h}}) + \sum_{\mathrm{h}=1}^{N} F_{\mathrm{f}} v_{\mathrm{s}\beta\mathrm{h}}\end{cases} \tag{20}$$

components, respectively. ω_{h} is the corresponding harmonic frequency. By substituting (15) into (7), the measured instantaneous power components P'_{s} and Q'_{s} can be expressed as follows,

$$\begin{aligned} P'_{\mathrm{s}} &= -\frac{3}{2}(\boldsymbol{i}_{\mathrm{sb}} \odot \boldsymbol{v}_{\mathrm{sb}} + \boldsymbol{i}_{\mathrm{sb}} \odot \boldsymbol{v}'_{\mathrm{sh}} + \boldsymbol{i}_{\mathrm{sh}} \odot \boldsymbol{v}_{\mathrm{sb}} + \boldsymbol{i}_{\mathrm{sh}} \odot \boldsymbol{v}'_{\mathrm{sh}}) \\ Q'_{\mathrm{s}} &= -\frac{3}{2}(\boldsymbol{i}_{\mathrm{sb}} \otimes \boldsymbol{v}_{\mathrm{sb}} + \boldsymbol{i}_{\mathrm{sb}} \otimes \boldsymbol{v}'_{\mathrm{sh}} + \boldsymbol{i}_{\mathrm{sh}} \otimes \boldsymbol{v}_{\mathrm{sb}} + \boldsymbol{i}_{\mathrm{sh}} \otimes \boldsymbol{v}'_{\mathrm{sh}}), \end{aligned} \tag{16}$$

where $\odot$ and $\otimes$ denote the dot product and cross product of two complex vectors.

The harmonic components $\boldsymbol{v}'_{\mathrm{sh}}$ in the voltage input $\boldsymbol{v}'_{\mathrm{s}}$ are filtered, and only account for a small proportion of $\boldsymbol{v}'_{\mathrm{s}}$. Therefore, $|\boldsymbol{v}'_{\mathrm{s}}|^2$ in the terms $B_\alpha, B_\beta, D_\alpha$ and D_β can be approximated as a dc value $|\boldsymbol{v}_{\mathrm{sb}}|^2$ at the operating point. The value is assumed to be pre-calculated as $|\boldsymbol{v}'_{\mathrm{s}}|^2 \approx v_{\mathrm{sb2}}$. Consequently, the terms B_α and B_β can then be linearized and expressed in terms of $\boldsymbol{v}'_{\mathrm{s}}$ as follows,

$$\begin{aligned} B_\alpha &\approx \frac{2P_{\mathrm{ref}}}{3v_{\mathrm{sb2}}} v'_{\mathrm{s}\alpha} + \frac{2Q_{\mathrm{ref}}}{3v_{\mathrm{sb2}}} v'_{\mathrm{s}\beta} \\ B_\beta &\approx \frac{2P_{\mathrm{ref}}}{3v_{\mathrm{sb2}}} v'_{\mathrm{s}\beta} - \frac{2Q_{\mathrm{ref}}}{3v_{\mathrm{sb2}}} v'_{\mathrm{s}\alpha} \end{aligned}. \tag{17}$$

For D_α and D_β, since $\boldsymbol{v}'_{\mathrm{sh}}$ is filtered, the dot product of two small quantities $\boldsymbol{i}_{\mathrm{sh}} \odot \boldsymbol{v}'_{\mathrm{sh}}$ and $\boldsymbol{i}_{\mathrm{sb}} \odot \boldsymbol{v}'_{\mathrm{sh}}$ are both small enough to be neglected. The measured P'_{s} in the integral sign can be approximated as constituted by the sum of the dot products $\boldsymbol{i}_{\mathrm{sb}} \odot \boldsymbol{v}_{\mathrm{sb}}$ and $\boldsymbol{i}_{\mathrm{sh}} \odot \boldsymbol{v}_{\mathrm{sb}}$. Equally, the measured Q'_{s} in the integral sign can be approximated as the sum of the cross products $\boldsymbol{i}_{\mathrm{sb}} \otimes \boldsymbol{v}_{\mathrm{sb}}$ and $\boldsymbol{i}_{\mathrm{sh}} \otimes \boldsymbol{v}_{\mathrm{sb}}$. Therefore, the approximations for P'_{s} and Q'_{s} can be written as,

$$\begin{aligned} P'_{\mathrm{s}} &\approx \underbrace{(-\frac{3}{2}\boldsymbol{i}_{\mathrm{sb}} \odot \boldsymbol{v}_{\mathrm{sb}})}_{P_{\mathrm{sdc}}} + \underbrace{(-\frac{3}{2}\boldsymbol{i}_{\mathrm{sh}} \odot \boldsymbol{v}_{\mathrm{sb}})}_{P_{\mathrm{sac}}} \\ Q'_{\mathrm{s}} &\approx \underbrace{(-\frac{3}{2}\boldsymbol{i}_{\mathrm{sb}} \otimes \boldsymbol{v}_{\mathrm{sb}})}_{Q_{\mathrm{sdc}}} + \underbrace{(-\frac{3}{2}\boldsymbol{i}_{\mathrm{sh}} \odot \boldsymbol{v}_{\mathrm{sb}})}_{Q_{\mathrm{sac}}} \end{aligned}, \tag{18}$$

where P_{sdc} and Q_{sdc} are the main dc components. P_{sac} and Q_{sac} are the main coupling ac components with oscillation frequency $\omega_{\mathrm{s}} - \omega_{\mathrm{h}}$. In this paper, the frequency-domain impedance modeling is designed for the VSC operating in steady-state. Therefore, it can be considered that the integral of dc components P_{sdc} and Q_{sdc} approximate the integral of reference value P_{sref} and Q_{sref} respectively in steady state, i.e., $\int P_{\mathrm{sdc}} \approx \int P_{\mathrm{sref}}$, $\int Q_{\mathrm{sdc}} \approx \int Q_{\mathrm{sref}}$, which has no effect on harmonic frequency domain analysis. By substituting (18) into (13), D_α and D_β can then be calculated as,

$$\begin{aligned} D_\alpha &\approx -\frac{2}{3}\frac{v'_{\mathrm{s}\alpha}Q_{\mathrm{sac}} - v'_{\mathrm{s}\beta}P_{\mathrm{sac}}}{v_{\mathrm{sb2}}(\omega_{\mathrm{s}}-\omega_{\mathrm{h}})} \approx -\sum_{\mathrm{h}=1}^{N}\frac{i_{\mathrm{s}\beta\mathrm{h}}}{\omega_{\mathrm{s}}-\omega_{\mathrm{h}}} \\ D_\beta &\approx -\frac{2}{3}\frac{v'_{\mathrm{s}\alpha}P_{\mathrm{sac}} - v'_{\mathrm{s}\beta}Q_{\mathrm{sac}}}{v_{\mathrm{sb2}}(\omega_{\mathrm{s}}-\omega_{\mathrm{h}})} \approx \sum_{\mathrm{h}=1}^{N}\frac{i_{\mathrm{s}\alpha\mathrm{h}}}{\omega_{\mathrm{s}}-\omega_{\mathrm{h}}} \end{aligned}. \tag{19}$$

The voltage control signal $\boldsymbol{v}'_{\mathrm{c}}$ can also be expressed as the sum of fundamental component and harmonic component as : $\boldsymbol{v}'_{\mathrm{c}} = \boldsymbol{v}_{\mathrm{cb}} + \boldsymbol{v}_{\mathrm{ch}}$. Therefore, by substituting (19) and (12) into (11), $\boldsymbol{v}_{\mathrm{ch}}$ can be calculated in terms of $\boldsymbol{v}_{\mathrm{sh}}$ and $\boldsymbol{i}_{\mathrm{sh}}$ as expressed in (20). The expression of $\boldsymbol{v}_{\mathrm{ch}}$ can further be expressed in the frequency-domain using the Laplace-transform as follows,

$$\begin{aligned} \begin{bmatrix} v_{\mathrm{c}\alpha\mathrm{h}} \\ v_{\mathrm{c}\beta\mathrm{h}} \end{bmatrix} &= \underbrace{\begin{bmatrix} L_{\mathrm{g}}K_{\mathrm{p}} & -\frac{K_{\mathrm{i}}L_{\mathrm{g}}}{\omega_{\mathrm{s}}-s/j} + \omega_{\mathrm{s}}L_{\mathrm{g}} \\ \frac{K_{\mathrm{i}}L_{\mathrm{g}}}{\omega_{\mathrm{s}}-s/j} - \omega_{\mathrm{s}}L_{\mathrm{g}} & L_{\mathrm{g}}K_{\mathrm{p}} \end{bmatrix}}_{\boldsymbol{Z}_{\mathrm{ci}}} \begin{bmatrix} i_{\mathrm{s}\alpha\mathrm{h}} \\ i_{\mathrm{s}\beta\mathrm{h}} \end{bmatrix} \\ &+ \underbrace{\begin{bmatrix} \frac{2P_{\mathrm{sref}}L_{\mathrm{g}}K_{\mathrm{p}}F_{\mathrm{f}}(s)}{3v_{\mathrm{sb2}}} + F_{\mathrm{f}}(s) & \frac{2L_{\mathrm{g}}K_{\mathrm{p}}Q_{\mathrm{sref}}F_{\mathrm{f}}(s)}{3v_{\mathrm{sb2}}} \\ -\frac{2L_{\mathrm{g}}K_{\mathrm{p}}Q_{\mathrm{sref}}F_{\mathrm{f}}(s)}{3v_{\mathrm{sb2}}} & \frac{2P_{\mathrm{sref}}L_{\mathrm{g}}K_{\mathrm{p}}F_{\mathrm{f}}(s)}{3v_{\mathrm{sb2}}} + F_{\mathrm{f}}(s) \end{bmatrix}}_{\boldsymbol{T}_{\mathrm{cv}}} \begin{bmatrix} v_{\mathrm{s}\alpha\mathrm{h}} \\ v_{\mathrm{s}\beta\mathrm{h}} \end{bmatrix} \end{aligned}, \tag{21}$$

where the transfer matrix of $\boldsymbol{i}_{\mathrm{sh}}$ and $\boldsymbol{v}_{\mathrm{sh}}$ to $\boldsymbol{v}_{\mathrm{ch}}$ are represented by $\boldsymbol{Z}_{\mathrm{ci}}$ and $\boldsymbol{T}_{\mathrm{cv}}$, respectively. The basic harmonic components relation of the VSC expressed in (1) can be written in the frequency domain by using Laplace transform as follows,

$$\begin{bmatrix} v_{\mathrm{s}\alpha\mathrm{h}} \\ v_{\mathrm{s}\beta\mathrm{h}} \end{bmatrix} = \underbrace{\begin{bmatrix} R_{\mathrm{g}} + sL_{\mathrm{g}} & 0 \\ 0 & R_{\mathrm{g}} + sL_{\mathrm{g}} \end{bmatrix}}_{\boldsymbol{Z}_{\mathrm{si}}} \begin{bmatrix} i_{\mathrm{s}\alpha\mathrm{h}} \\ i_{\mathrm{s}\beta\mathrm{h}} \end{bmatrix} + \begin{bmatrix} v_{\mathrm{c}\alpha\mathrm{h}} \\ v_{\mathrm{c}\beta\mathrm{h}} \end{bmatrix}. \tag{22}$$

By substituting (21) into (22), the impedance model of VM-DPC based VSC in the harmonic frequency domain can be calculated as,

$$\begin{bmatrix} v_{\mathrm{s}\alpha\mathrm{h}} \\ v_{\mathrm{s}\beta\mathrm{h}} \end{bmatrix} = \underbrace{(\boldsymbol{I} - \boldsymbol{T}_{\mathrm{cv}})^{-1}(\boldsymbol{Z}_{\mathrm{si}} + \boldsymbol{Z}_{\mathrm{ci}})}_{\boldsymbol{Z}_{\mathrm{VSC}}} \begin{bmatrix} i_{\mathrm{s}\alpha\mathrm{h}} \\ i_{\mathrm{s}\beta\mathrm{h}} \end{bmatrix}, \tag{23}$$

where $\boldsymbol{Z}_{\mathrm{VSC}}$ represents the final impedance matrix of VSC with DPC in the $\alpha\beta$- reference frame.

B. Error Analysis

Since $|\boldsymbol{v}'_{\mathrm{s}}|^2$ is considered as ${v'_{\mathrm{s}\alpha}}^2 + {v'_{\mathrm{s}\beta}}^2$, while the harmonic is large, there will be large ripples with harmonic frequency in term $|\boldsymbol{v}_{\mathrm{s}}|^2$ as,

$$
\begin{aligned}
|\boldsymbol{v}_{\mathrm{s}}'|^2 =& {v_{\mathrm{s}\alpha}'}^2 + {v_{\mathrm{s}\beta}'}^2 = \underbrace{|\boldsymbol{v}_{\mathrm{sb}}|^2 + \sum_{\mathrm{h}=1}^{N} |F_{\mathrm{f}}\boldsymbol{v}_{\mathrm{sh}}|^2}_{\text{with zero frequency}} \\
&+ \underbrace{v_{\mathrm{s}\alpha\mathrm{b}} \sum_{\mathrm{h}=1}^{N} F_{\mathrm{f}} v_{\mathrm{s}\alpha\mathrm{h}} + v_{\mathrm{s}\beta\mathrm{b}} \sum_{\mathrm{h}=1}^{N} F_{\mathrm{f}} v_{\mathrm{s}\beta\mathrm{h}}}_{\text{coupled with fundamental component}} \\
&+ \underbrace{\sum_{\mathrm{h}=1}^{N}\sum_{\mathrm{i}=1}^{N} (F_{\mathrm{f}} v_{\mathrm{s}\alpha\mathrm{h}} F_{\mathrm{f}} v_{\mathrm{s}\alpha i} + F_{\mathrm{f}} v_{\mathrm{s}\beta\mathrm{h}} F_{\mathrm{f}} v_{\mathrm{s}\beta i}) | (h \neq i)}_{\text{negligible}}
\end{aligned}
\tag{24}
$$

In the off-line theoretical analysis, it is assumed that the system is working at an operating point as $|\boldsymbol{v}_{\mathrm{s}}'|^2 \approx v_{\mathrm{sb2}}$. The BPF can primarily reduce the error between v_{sb2} and the actual value of $|\boldsymbol{v}_{\mathrm{s}}|^2$ under the situation with relatively small voltage harmonic distortion. The accuracy of the proposed impedance modeling method and the effectiveness of integral part approximation used in (19) is verified by a point-by-point frequency scanning, where the results are results presented in the next section.

IV. Matrix Transformation and Stability Criteria

The impedance analysis of VSC with the VM-DPC by using a SISO Nyquist stability criteria is discussed in this section. The impedance matrix in $\alpha\beta$ reference frame is transformed into a diagonal impedance matrix in the sequence-domain by using the method proposed in [15], [16]. Therefore, the stability can be easily estimated by using a simple SISO Nyquist stability criteria.

Generally speaking, a 2×2 transfer matrix can be transformed to an expression in terms of the corresponding complex space vector and its conjugate. The impedance matrix $\boldsymbol{Z}_{\mathrm{VSC}}$ deduced in (23) can be considered as a general $\alpha\beta$ impedance matrix written as follows,

$$
\begin{bmatrix} v_{\mathrm{s}\alpha\mathrm{h}} \\ v_{\mathrm{s}\beta\mathrm{h}} \end{bmatrix} = \boldsymbol{Z}_{\mathrm{vsc}} \begin{bmatrix} i_{\mathrm{s}\alpha\mathrm{h}} \\ i_{\mathrm{s}\beta\mathrm{h}} \end{bmatrix}, \boldsymbol{Z}_{\mathrm{vsc}} = \begin{bmatrix} Z_{\alpha\alpha}(s) & Z_{\alpha\beta}(s) \\ Z_{\beta\alpha}(s) & Z_{\beta\beta}(s) \end{bmatrix}. \tag{25}
$$

The equivalent equation of (25) can be derived in the following,

$$
\boldsymbol{v}_{\mathrm{sh}} = Z_{\mathrm{VSC,p}}(s)\boldsymbol{i}_{\mathrm{sh}} + Z_{\mathrm{VSC,n}}(s)\boldsymbol{i}_{\mathrm{sh}}^*, \tag{26}
$$

where $\boldsymbol{v}_{sh} = v_{\mathrm{s}\alpha\mathrm{h}} + jv_{\mathrm{s}\beta\mathrm{h}}$, $\boldsymbol{i}_{sh} = i_{\mathrm{s}\alpha\mathrm{h}} + ji_{\mathrm{s}\beta\mathrm{h}}$, $Z_{\mathrm{VSC,p}}(s)$ and $Z_{\mathrm{VSC,n}}(s)$ are the equivalent transfer functions of the sequence-domain impedance, which can be derived as,

$$
\begin{aligned}
Z_{\mathrm{VSC,p}}(s) &= \frac{Z_{\alpha\alpha}(s) + Z_{\beta\beta}(s)}{2} + j\frac{Z_{\beta\alpha}(s) - Z_{\alpha\beta}(s)}{2} \\
Z_{\mathrm{VSC,n}}(s) &= \frac{Z_{\alpha\alpha}(s) - Z_{\beta\beta}(s)}{2} + j\frac{Z_{\beta\alpha}(s) + Z_{\alpha\beta}(s)}{2}
\end{aligned}. \tag{27}
$$

Due to the symmetrical characteristic of the impedance matrix, i.e., $Z_{\alpha\alpha}(s) = Z_{\beta\beta}(s)$, $Z_{\beta\alpha}(s) = -Z_{\alpha\beta}(s)$, it can be deduced that $Z_{\mathrm{VSC,n}}(s) = 0$, which implies that the positive sequence voltage will not induce negative sequence current, and the negative sequence voltage will not be inducted into the grid without negative-sequence harmonic content. Therefore, in this case, the system is transformed into a SISO system with only $Z_{\mathrm{VSC,p}}(s)$, which needs to be considered. Consequently, the corresponding frequency scanning verification of the impedance model and the stability analysis of DPC based VSC with the proposed method can be considerably simplified.

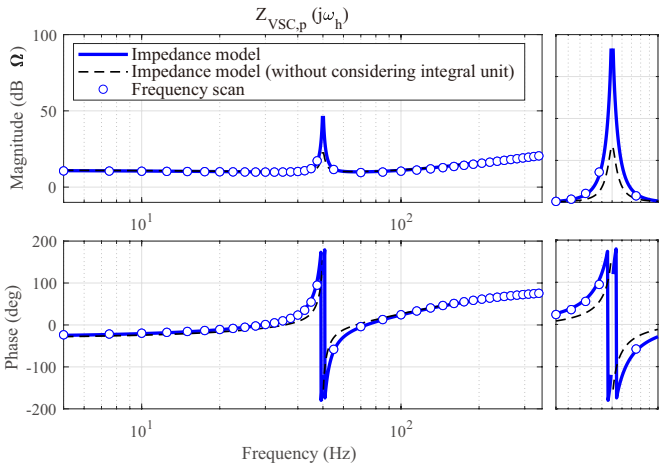

Fig. 2. Comparison of positive-sequence impedance calculated by proposed method and point-by-point frequency simulation analyzing the system specified in Table I. ($K_{\mathrm{p}} = 500, K_{\mathrm{i}} = 10000$)

The accuracy of $Z_{\mathrm{VSC,p}}(s)$ is verified by a point-by-point frequency scan approach with the control parameters ($K_{\mathrm{p}} = 500$, $K_{\mathrm{i}} = 10000$) carried out in Matlab/Simulink, as shown in Fig. 2. The parameters of the VSC are presented in Table I. The voltage perturbation are injected with harmonic frequency 2.5 Hz–47.5 Hz and 55 Hz–305 Hz with an interval of 2.5 Hz and 20 Hz, respectively. The value of the perturbation is set at 0.02 pu, which is small enough to maintain the system in steady state but large enough for the system impedance identification. The enlarged windows near synchronous frequency ω_{s} (50 Hz) is shown at the right of Fig. 2, where the black dotted line represents the model without considering the integral term of the PI unit, i.e., $D_\alpha = 0$, $D_\beta = 0$. The enlarged window shows that the integral term mainly affects the frequency-response of VSC near the synchronous frequency. The consideration of the integral control (19) can effectively improve the precision of the impedance model. Fig. 2 shows a satisfactory conformity between $Z_{\mathrm{VSC,p}}(s)$ calculated by the proposed impedance modeling method and the point-by-point frequency-scan results.

Assuming the weak-grid impedance is balanced. The impedance can be calculated as follows,

$$
Z_{\mathrm{grid}}(s) = \frac{L_{\mathrm{n}}s + R_{\mathrm{n}}}{(L_{\mathrm{n}}s + R_{\mathrm{n}})C_{\mathrm{n}}s + 1}, \tag{28}
$$

where R_{n} is the grid resistance, L_{n} is the grid series inductance and C_{n} is the parallel capacitor as shown in Fig. 1. The stability of the grid-connected VSC can be estimated by using the Nyquist stability criterion proposed in [6]. The frequency response of the system including VSC and weak grid is represented by a Thevenin equivalent circuit consisting of the positive-sequence impedance $Z_{\mathrm{VSC,p}}$ in series with the grid

TABLE I
PARAMETERS OF SIMULATED GRID-CONNECTED VSC SYSTEM AND VM-DPC CONTROLLER

Parameter	Symbol	Value	Unit
Rated power	P_{ref}	2.5	kW
Switching frequency	f_{w}	4	kHz
Sampling frequency	f_{sa}	4	kHz
Fundamental frequency	f	50	Hz
Ground-to-line Voltage	$v_{\text{s,rms}}$	110	V
Natural frequency of BPF	ω_{fn}	50	Hz
Damping ratio of BPF	ζ_{f}	0.1	
Dc voltage	v_{dc}	730	V
VSC resistance	R_{g}	0.12	Ω
VSC inductor	L_{g}	6	mH
Line resistance	R_{n}	0.5	Ω
Line inductance	L_{n}	10	mH
Line capacitance	C_{n}	15	μF
Short Circuit Ratio	SCR	4.6	
Control Parameters			
Parameter	Value	Parameter	Value
K_{p}	1000	K_{i}	10000

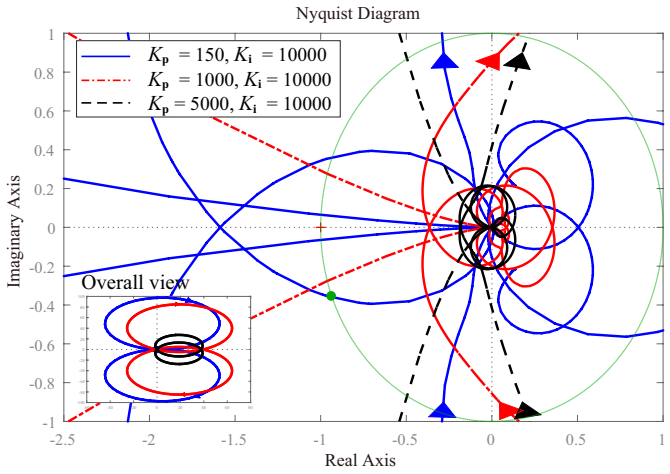

Fig. 3. Nyquist diagram of $G_{\alpha\beta}(s)$ with different K_{p} and fixed K_{i}.

impedance Z_{grid}. The stability of the system can be identified by the eigenvalues of the transfer function given as,

$$H_{\text{s}} = \frac{1}{1 + G_{\alpha\beta}(s)}, \tag{29}$$

where $G_{\alpha\beta}(s) = Z_{\text{grid}}(s)/Z_{\text{VSC,p}}(s)$ is the feedback characteristic equation of the system. Based on the linear-control theory that the closed-loop transfer function H_{s} guarantees stable operation only if $G_{\alpha\beta}(s)$ satisfies the Nyquist stability criterion.

V. SIMULATION AND CASE STUDIES

The case studies based on a simulation model built in Matlab/Simulink SimScape Power System are carried out in this section to further verify the effectiveness of the proposed impedance modeling on VSC with the VM-DPC. The parameters of VSC and the grid impedance are presented in Table I. In [30], the VM-DPC method of VSC has already verified the effectiveness and stability in a weak-grid through the experimental prototype. However, the control parameters on the control effect are not thoroughly discussed. Therefore, in this paper, we mainly focus on the influence of the control parameters K_{p} and K_{i} on the stability. The system performances under the different grid SCR values are also studied. It should be noted that the selection of control parameters in this paper mainly depends on the verification of the proposed impedance model, which is not optimal for the control effect.

A. Effect of K_{p} on System Performance

The stability of the grid-connected VSC can be identified by applying the Nyquist stability analysis on $G_{\alpha\beta}(s)$. The Nyquist diagrams of the system and their zoomed-in view near the critical point (-1,0) with three different control parameter settings are shown in Fig. 3. It can be seen that the characteristic loci of $G_{\alpha\beta}(s)$ with $K_{\text{p}} = 5000$ and $K_{\text{p}} = 1000$ will not encircle the critical point which means the system is stable. If K_{p} decreases to 150, the characteristic loci will encircle the

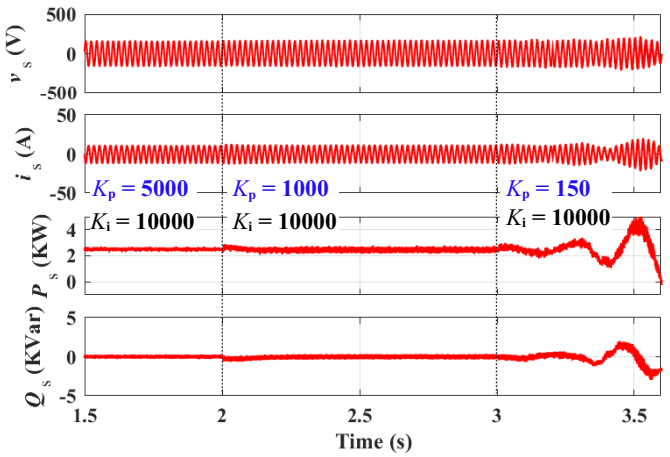

Fig. 4. Comparison of system performance with different K_{p} and fixed K_{i}.

critical point will intersect with the unit circle at the frequency harmonic point 52.2 Hz. The analysis indicates that the system becomes unstable at a lower K_{p} value. However, it should be noted that if the value of K_{p} is too high, sizable harmonic content may come with the measurement and modulation. Therefore, a compromise is needed when choosing a proper value of K_{p}.

Fig. 4 shows the simulation result of the system performance with different K_{p} values. It is shown that the system with $K_{\text{p}} = 5000$ is stable before 2 s. The system can still operate in steady state after a step change of the control parameter K_{p} from 5000 to 1000 at 2 s. However, the system becomes unstable and starts to oscillate when K_{p} decreases to 150 at 3 s. The frequency of the main oscillating component in the output current is 52.5 Hz, which is close to the frequency of intersection point calculated by the Nyquist analysis shown in Fig. 3. Consequently, it can be concluded that the Nyquist analysis shows consistency with the simulation results. Therefore, the proposed impedance analysis method is effective and accurate.

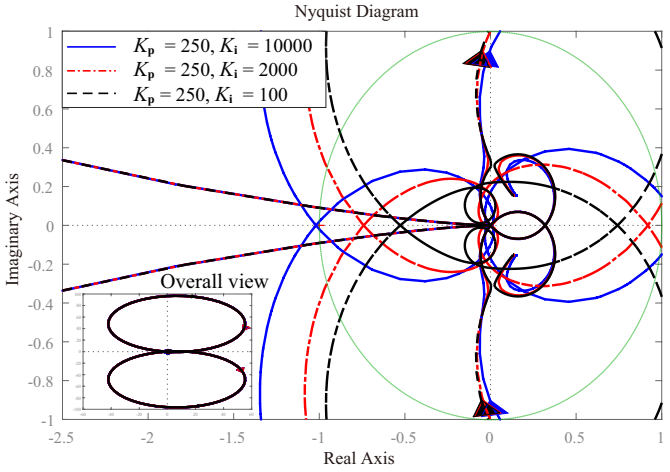

Fig. 5. Nyquist diagram of $G_{\alpha\beta}(s)$ with different control parameter K_i when K_p is fixed.

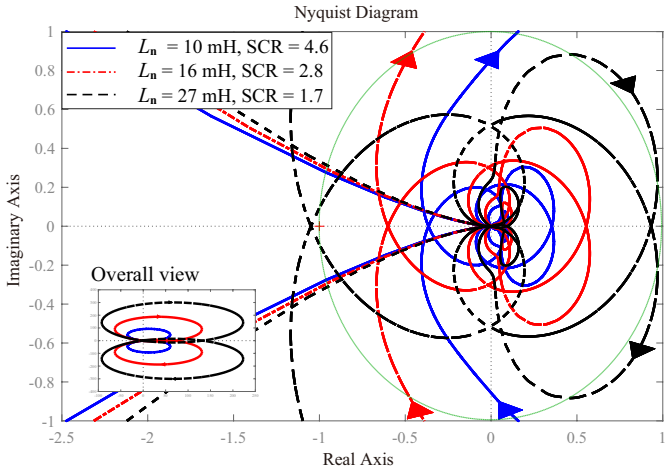

Fig. 7. Nyquist diagram of $G_{\alpha\beta}(s)$ with fixed control parameters ($K_\mathrm{p} = 1000, K_\mathrm{i} = 10000$) under different grid conditions.

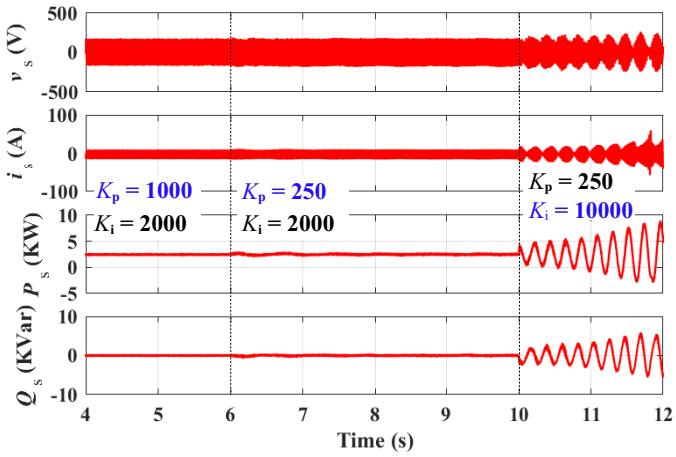

Fig. 6. Comparison of system response with different control parameters settings.

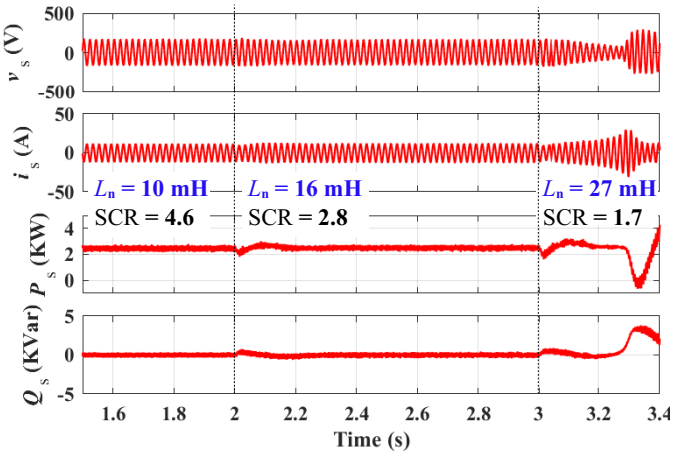

Fig. 8. Comparison of system performance with variation of grid inductance L_n with fixed control parameter ($K_\mathrm{p} = 1000, K_\mathrm{i} = 10000$).

B. Effect of K_i on System Performance

Fig. 5 shows the Nyquist diagram of the system with different K_i values when K_p is set to 250. The result is consistent with the conclusion obtained in Section IV, that the effect of the integral unit on impedance characteristics is limited. It is observed that the characteristic loci encircle the critical point when K_i increases from 100 to 10000. It indicates the system becomes unstable. The frequency of the point of intersection between the characteristic loci and the unit circle is 53.9 Hz.

The time-domain simulation results shown in Fig. 6 present the system responses using different control parameters. The system returns to the steady-state shortly when K_p changes from 1000 to 250 and $K_\mathrm{i} = 2000$. The system turns unstable and starts to oscillate when K_i changes from 2000 to 10000. The frequency of the main oscillation component calculated by the FFT analysis is 55 Hz, which is consistent with the Nyquist diagram shown in Fig. 5. Consequently, the effectiveness of proposed modeling is verified, and it can be concluded that although K_p is the main influencing factor of impedance characteristic, the increase of K_i may also decrease the system stability with a relatively low value of K_p.

C. Effect of SCR on System Performance

The Nyquist diagrams of the VSC connected to different grid conditions are shown in Fig. 7. The control parameters are set to $K_\mathrm{p} = 1000, K_\mathrm{i} = 10000$ in this study case. It can be observed that the characteristic loci of $G_{\alpha\beta}(s)$ is far from the critical point under the grid condition with SCR = 4.6. The loci moves close to the critical point with the when the grid inductance increases and the SCR decreases from 4.6 to 2.8. The characteristic loci encircles the critical point under the grid of SCR = 1.7. The results indicate that the time-domain response of the weak-grid connected VSC system with SCR = 1.7 will be unstable.

A time-domain simulation is carried out, as shown in Fig. 8. Two inductances with the same value of 6 mH are connected in series to the grid impedance at 2 s and 3 s, respectively. It

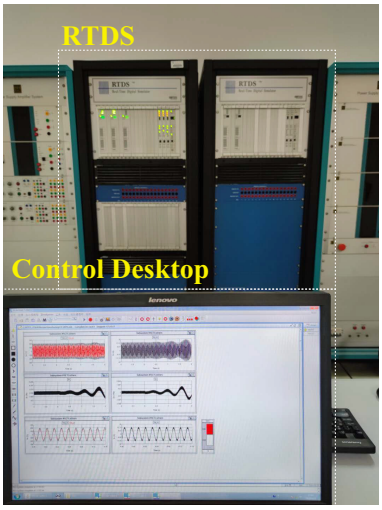

Fig. 9. HIL test setup with RTDS

is shown that the system returns to steady-state shortly after the SCR reduced to 2.8 at 2 s. The system becomes unstable and starts to oscillate once the system SCR reduces to 1.7 at 3 s. Simulation results show consistency with the proposed impedance analysis results. Consequently, it can be concluded that the increase of grid inductance and grid SCR will result in system instability.

VI. HIL TEST

In this section, a prototype of grid-connected VSC using VM-DPC is tested through an HIL test system shown in Fig. 9. The parameters of the VM-DPC and the grid impedance can be changed through communications with a control laptop. The grid-connected VSC using the VM-DPC and the grid impedance are represented by detailed EMT models in the RTDS. To verify the simulation results, the parameters of the grid and VSC are chosen to be the same as the simulation being presented in Table. I and two different cases are carried out as follows.

Case A: In this case, the influence of the variation of control parameter K_{p} on system stability is investigated. The rated power of the VSC is set to 2.5 kW, and the grid parameters are fixed as $L_{\mathrm{n}} = 10$ mH, $R_{\mathrm{n}} = 0.5\ \Omega$ (SCR = 4.6). Initially, the control parameters are set to ($K_{\mathrm{p}} = 1000$, $K_{\mathrm{i}} = 10000$). From Fig. 10, it can be observed that the system is operating normally in steady-state from 5 s to 6 s. Then, at 6 s, the K_{p} is decreased from 1000 to 50. The decreasing of K_{p} excites an oscillation in the stator current and power components, and the system becomes unstable. The results show the consistency with Fig. 4 and verify the conclusions drawn in Section V-A.

Case B: The influence of grid impedance on the system stability is investigated in this case study. The control parameters are fixed as $K_{\mathrm{p}} = 1000$, $K_{\mathrm{i}} = 10000$. Initially, the grid impedance is set to $L_{\mathrm{n}} = 10$ mH, $R_{\mathrm{n}} = 0.5\ \Omega$ (SCR = 4.6). Then, at 6 s, an inductance with $L_{\mathrm{n}} = 6$ mH is set in series into the grid impedance to decrease the system SCR from 4.6 to 2.8. It can be observed from Fig. 11 that after experiencing a system transient dynamics about 1 s, the system returns to

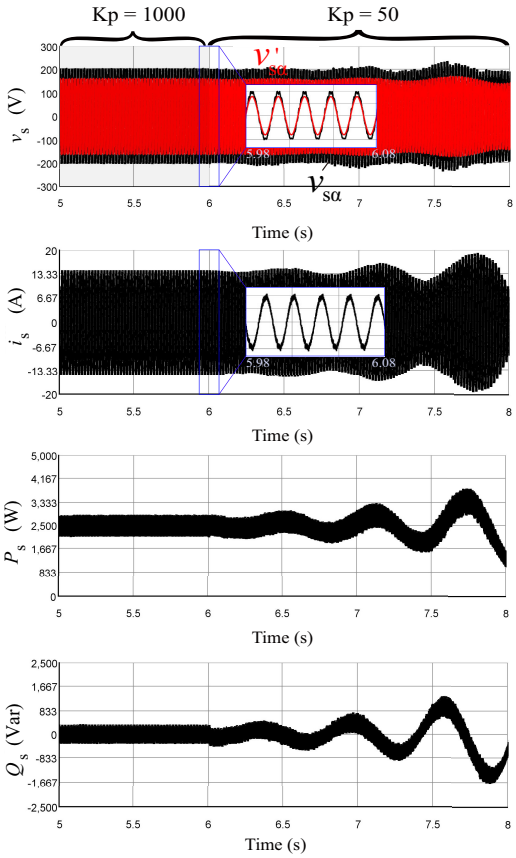

Fig. 10. System performance under different values and fixed grid impedance ($L_{\mathrm{n}} = 10$ mH, $R_{\mathrm{n}} = 0.5\ \Omega$) in a HIL test.

steady-state. The result indicates that the system can operate normally under the grid condition with SCR = 2.8, which show consistency with the conclusions drawn in Section V-C.

VII. CONCLUSION

An impedance modeling approach and a stability analysis method of grid-connected VSC using DPC was developed. The impedance matrix was firstly built in $\alpha\beta-$ reference frame and transformed into a positive-sequence impedance. The stability of the system was analysed by a SISO Nyquist stability criterion. The influences of the control parameters and the SCR of the grid on the system stability were discussed. The results show that the stability of weak-grid connected VSC with DPC is mainly related to the value of the proportional control parameter. The reduction of both proportional and integral control parameters will reduce the system stability. The influence of the integral parameter on the impedance characteristic mainly embodies near nominal frequency and has only a limited effect on system stability. Also, the analysis verifies that a decrease in grid SCR will deteriorates the system stability performance. The simulation and HIL tests verify the effectiveness of the proposed method. Consequently, the proposed modeling approach fills the gap of analyzing the harmonic interaction between DPC based VSC and weak grid. Impedance characteristics obtained from the proposed impedance modeling method offer an excellent basis for control parameter design of DPC for VSC.

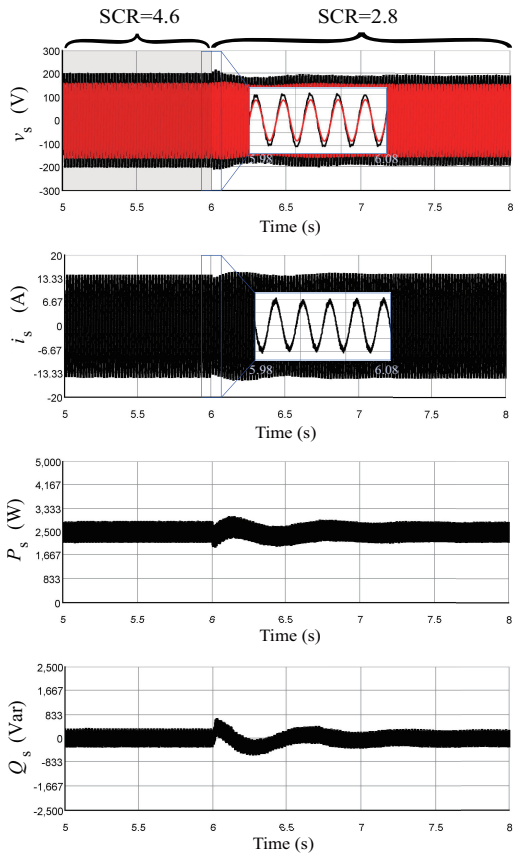

Fig. 11. System performance under different grid SCR values and fixed control parameters ($K_\mathrm{p} = 1000$, $K_\mathrm{i} = 10000$) in a HIL test

APPENDIX

The authors would like to thank the National Key R&D Program of China (2018YFB0904004) for the financial support. They would also like to thank Dr. Peng Wang from the Department of Sustainable Electric Networks and Sources of Energy, Technische Universität Berlin, for proofreading the paper.

REFERENCES

[1] F. Blaabjerg, R. Teodorescu, S. Member, M. Liserre, A. V. Timbus, and S. Member, "Overview of control and grid synchronization for distributed power generation systems," *IEEE Trans. Ind. Electron.*, vol. 53, no. 5, pp. 1398–1409, 2006.

[2] W. Cao, Y. Ma, and F. Wang, "Sequence-impedance-based harmonic stability analysis and controller parameter design of three-phase inverter-based multibus AC power systems," *IEEE Trans. Power Electron.*, vol. 32, no. 10, pp. 7674–7693, 2017.

[3] L. Harnefors, "Modeling of three-phase dynamic systems using complex transfer functions and transfer matrices," *IEEE Trans. Ind. Electron.*, vol. 54, no. 4, pp. 2239–2248, 2007.

[4] L. Harnefors, M. Bongiorno, and S. Lundberg, "Input-admittance calculation and shaping for controlled voltage-source converters," *IEEE Trans. Ind. Electron.*, vol. 54, no. 6, pp. 3323–3334, 2007.

[5] Jian Sun, "Impedance-based stability criterion for grid-connected inverters," *IET Power Electron.*, vol. 26, no. 11, pp. 1–10, 2011.

[6] M. Cespedes and J. Sun, "Impedance modeling and analysis of grid-connected voltage-source converters," *IET Power Electron.*, vol. 29, no. 3, pp. 1254–1261, 2014.

[7] M. K. Bakhshizadeh, S. Member, F. Blaabjerg, and J. Hjerrild, "Improving the impedance-based stability criterion by using the vector fitting method," *IEEE Trans. Energy Convers.*, vol. 33, no. 4, pp. 1739–1747, 2018.

[8] Z. Miao, "Impedance-model-based SSR analysis for type 3 wind generator and series-compensated network," *IEEE Trans. Energy Convers.*, vol. 27, no. 4, pp. 984–991, 2012.

[9] K. M. Alawasa, Y. A. R. I. Mohamed, and W. Xu, "Modeling, analysis, and suppression of the impact of full-scale wind-power converters on subsynchronous damping," *IEEE Syst. J.*, vol. 7, no. 4, pp. 700–712, 2013.

[10] M. Amin and M. Molinas, "Understanding the origin of oscillatory phenomena observed between wind farms and HVDC systems," *IEEE J. Emerg. Sel. Top. Power Electron.*, vol. 5, no. 1, pp. 378–392, 2017.

[11] H. Liu, X. Xie, S. Member, and Z. Liu, "Comparative studies on the impedance models of VSC-based renewable generators for SSI stability analysis," *IEEE Trans. Energy Convers.*, vol. 34, no. 3, pp. 1442–1453, 2019.

[12] M. Berg, A. Aapro, R. Luhtala, and T. Messo, "Small-signal analysis of photovoltaic inverter with impedance-compensated phase-locked loop in weak grid," *IEEE Trans. Energy Convers.*, vol. 35, no. 1, pp. 347–355, 2020.

[13] C. Zhang, X. Cai, M. Molinas, and A. Rygg, "On the impedance modeling and equivalence of AC/DC-side stability analysis of a grid-tied type-IV wind turbine system," *IEEE Trans. Energy Convers.*, vol. 34, no. 2, pp. 1000–1009, 2019.

[14] B. Wen, D. Boroyevich, R. Burgos, P. Mattavelli, and Z. Shen, "Analysis of D-Q small-signal impedance of grid-tied inverters," *IEEE Trans. Power Electron.*, vol. 31, no. 1, pp. 675–687, 2016.

[15] S. Shah and L. Parsa, "Impedance modeling of three-phase voltage source converters in dq, sequence, and phasor domains," *IEEE Trans. Energy Convers.*, vol. 32, no. 3, pp. 1139–1150, 2017.

[16] X. Wang, L. Harnefors, and F. Blaabjerg, "Unified impedance model of grid-connected voltage-source converters," *IEEE Trans. Power Electron.*, vol. 33, no. 2, pp. 1775–1787, 2018.

[17] B. Wen, D. Boroyevich, R. Burgos, P. Mattavelli, and Z. Shen, "Inverse Nyquist stability criterion for grid-tied inverters," *IEEE Trans. Power Electron.*, vol. 32, no. 2, pp. 1548–1556, 2017.

[18] L. Xu, H. Xin, L. Huang, H. Yuan, P. Ju, and D. Wu, "Symmetric admittance modeling for stability analysis of grid-connected converters," *IEEE Trans. Energy Convers.*, vol. 35, no. 1, pp. 434–444, 2020.

[19] D. Yang, X. Wang, F. Liu, K. Xin, Y. Liu, and F. Blaabjerg, "Symmetrical pll for siso impedance modeling and enhanced stability in weak grids," *IEEE Trans. Power Electron.*, vol. 35, no. 2, pp. 1–1, 2019.

[20] Y. Liao and X. Wang, "Stationary-frame complex-valued frequency-domain modeling of three-phase power converters," *IEEE J. Emerg. Sel. Top. Power Electron.*, vol. 8, no. 2, pp. 1–1, 2019.

[21] J. Liu, X. Du, Y. Shi, and H.-M. Tai, "Impedance measurement of three-phase inverter in the stationary frame using frequency response analyzer," *IEEE Trans. Power Electron.*, vol. 35, no. 9, pp. 1–1, 2020.

[22] T. Noguchi, H. Tomiki, S. Kondo, and I. Takahashi, "Direct power control of PWM converter without power-source voltage sensors," *IEEE Trans. Ind. Appl.*, vol. 34, no. 3, pp. 473–479, 1998.

[23] M. Malinowski, M. Jasiński, and M. P. Kazmierkowski, "Simple direct power control of three-phase PWM rectifier using space-vector modulation (DPC-SVM)," *IEEE Trans. Ind. Electron.*, vol. 51, no. 2, pp. 447–454, 2004.

[24] J. Hu and B. Hu, "Direct active and reactive power regulation of grid connected voltage source converters using sliding mode control approach," *IEEE Trans. Energy Convers.*, vol. 25, no. 4, pp. 1028–1039, 2010.

[25] Y. Gui, C. Kim, and C. C. Chung, "Grid voltage modulated direct power control for grid connected voltage source inverters," *Int. J. Control. Autom. Syst.*, vol. 15, no. 5, pp. 2078–2084, 2017.

[26] Y. Gui, M. Li, J. Lu, S. Golestan, J. M. Guerrero, and J. C. Vasquez, "A voltage modulated DPC approach for three-phase PWM rectifier," *IEEE Trans. Ind. Electron.*, vol. 65, no. 10, pp. 7612–7619, 2018.

[27] S. Mensou, A. Essadki, T. Nasser, and B. B. Idrissi, "A direct power control of a DFIG based-WECS during symmetrical voltage dips," *Prot. Control Mod. Power Syst.*, vol. 5, no. 1, p. 5, 2020.

[28] S. Boubzizi, H. Abid, A. El, and M. Chaabane, "Comparative study of three types of controllers for DFIG in wind energy conversion system," *Prot. Control Mod. Power Syst.*, vol. 3, no. 3, pp. 214–225, 2018.

[29] S. El Daoudi, L. Lazrak, and M. Ait Lafkih, "Sliding mode approach applied to sensorless direct torque control of cage asynchronous motor via multi-level inverter," *Prot. Control Mod. Power Syst.*, vol. 5, no. 1, 2020.

[30] Y. Gui, X. Wang, H. Wu, and F. Blaabjerg, "Voltage-modulated direct power control for a weak grid-connected voltage source inverters," *IEEE Trans. Power Electron.*, vol. 34, no. 11, pp. 11383–11395, 2019.

[31] Y. Gui, X. Wang, F. Blaabjerg, and D. Pan, "Control of grid-connected voltage-source converters: the relationship between direct-power control and vector-current control," *IEEE Ind. Electron. Mag.*, vol. 13, pp. 31–40, June 2019.
[32] Y. Gui, C. Kim, C. C. Chung, J. M. Guerrero, Y. Guan, and J. C. Vasquez, "Improved direct power control for grid-connected voltage source converters," *IEEE Trans. Ind. Electron.*, vol. 65, no. 10, pp. 8041–8051, 2018.
[33] Y. Gui, X. Wang, and F. Blaabjerg, "Vector current control derived from direct power control for grid-connected inverters," *IEEE Trans. Power Electron.*, vol. 34, no. 9, pp. 9224–9235, 2019.
[34] Y. Gui, F. Blaabjerg, X. Wang, J. Bendtsen, D. Yang, and J. Stoustrup, "Improved dc-link voltage regulation strategy for grid-connected converters," *IEEE Trans. Ind. Electron.*, 2020, to be published, doi: 10.1109/TIE.2020.2989720.
[35] H. Akagi, Y. Kanazawa, and A. Nabae, "Instantaneous reactive power compensators comprising switching devices without energy storage components," *IEEE Trans. Ind. Appl.*, vol. IA-20, no. 3, pp. 625–630, 1984.

Shuning Gao (S'17) received the B.S. degree in electrical engineering from Huazhong University of Science and Technology, Wuhan, China, in 2015. He is currently working toward the Ph.D. degree in the Shandong University.

In December 2019, he was a visiting student with the Automation & Control Section, Department of Electronic Systems, Aalborg University. His research interests include modeling and control of power electronics, stability analysis of power electronics based power systems.

Haoran Zhao (S'12-M'15) received the B.E. degree from Shandong University, China, in 2005, the M.E. degree from the Technical University of Berlin, Germany, in 2009, and the Ph.D. degree from Technical University of Denmark, Denmark, in 2014. Currently, he is a professor with the School of Electrical Engineering, Shandong University, China.

He was an Electrical Engineer with State Grid Corporation of China (SGCC), in 2005. From 2010 to 2011, he worked as an Application Developer in DIgSILENT GmbH, Germany. His research interests include modeling and integration study of wind power, control of energy storage system, and integrated energy systems.

Yonghao Gui (S'11-M'17-SM'20) received the B.S. degree in automation from Northeastern University, Shenyang, China, in 2009, and the M.S. and Ph.D. degrees in electrical engineering from Hanyang University, Seoul, South Korea, in 2012 and 2017, respectively.

From Feb. 2017 to Nov. 2018, he worked with the Department of Energy Technology, Aalborg University, Aalborg, Denmark, as a Postdoctoral Researcher. Since Dec. 2018, he has been working with the Automation & Control Section, Department of Electronic Systems, Aalborg University, Aalborg, Denmark, where he is currently an Assistant Professor. His research interests include Control of Power Electronics in Power Systems, Energy Internet, and Smart Grids.

Dr. Gui has served as an Associate Editor for the IEEE ACCESS and the International Journal of Control, Automation and Systems (IJCAS). He was a recipient of the IEEE Power & Energy Society General Meeting Best Conference Paper Award in 2019 the IJCAS Academic Activity Award 2019.

Jia Luo (S'17) received the B.S. degree in electrical engineering from Huazhong University of Science and Technology, Wuhan, China, in 2015 and the M.S. degree in electrical engineering from Shandong University, Jinan, China, in 2020. He is currently working toward the Ph.D. degree in Shandong University. His research interests include modeling and control of DFIG, LVRT strategy of DFIG, and voltage stability analysis.

Frede Blaabjerg (S'86–M'88–SM'97–F'03) was with ABB-Scandia, Randers, Denmark, from 1987 to 1988. From 1988 to 1992, he got the PhD degree in Electrical Engineering at Aalborg University in 1995. He became an Assistant Professor in 1992, an Associate Professor in 1996, and a Full Professor of power electronics and drives in 1998. From 2017 he became a Villum Investigator. He is honoris causa at University Politehnica Timisoara (UPT), Romania and Tallinn Technical University (TTU) in Estonia.

His current research interests include power electronics and its applications such as in wind turbines, PV systems, reliability, harmonics and adjustable speed drives. He has published more than 600 journal papers in the fields of power electronics and its applications. He is the co-author of four monographs and editor of ten books in power electronics and its applications.

He has received 32 IEEE Prize Paper Awards, the IEEE PELS Distinguished Service Award in 2009, the EPE-PEMC Council Award in 2010, the IEEE William E. Newell Power Electronics Award 2014, the Villum Kann Rasmussen Research Award 2014, the Global Energy Prize in 2019 and the 2020 IEEE Edison Medal. He was the Editor-in-Chief of the IEEE TRANSACTIONS ON POWER ELECTRONICS from 2006 to 2012. He has been Distinguished Lecturer for the IEEE Power Electronics Society from 2005 to 2007 and for the IEEE Industry Applications Society from 2010 to 2011 as well as 2017 to 2018. In 2019-2020 he serves a President of IEEE Power Electronics Society. He is Vice-President of the Danish Academy of Technical Sciences too. He is nominated in 2014-2019 by Thomson Reuters to be between the most 250 cited researchers in Engineering in the world.